

MOX–Report No. 24/2013

**SPEED-Spectral Elements in Elastodynamics with
Discontinuous Galerkin: a non-conforming approach
for 3D multi-scale problems**

MAZZIERI, I.; STUPAZZINI, M.; GUIDOTTI, R.; SMERZINI,
C.

MOX, Dipartimento di Matematica “F. Brioschi”
Politecnico di Milano, Via Bonardi 9 - 20133 Milano (Italy)

mox@mate.polimi.it

<http://mox.polimi.it>

SPEED-SPECTRAL ELEMENTS IN ELASTODYNAMICS WITH DISCONTINUOUS GALERKIN: A NON-CONFORMING APPROACH FOR 3D MULTI-SCALE PROBLEMS

I. MAZZIERI¹, M. STUPAZZINI², R. GUIDOTTI³, C. SMERZINI³

May 2, 2013

¹ MOX–Laboratory for Modeling and Scientific Computing
Department of Mathematics, Politecnico di Milano
P.za Leonardo da Vinci 32, 20133 Milan, IT.
ilario.mazzieri@mail.polimi.it

² Munich RE - Geo Risk Königinstr. 107, 80802 Munich, D.
mstupazzini@munichre.com

³ Department of Civil and Environmental Engineering, Politecnico di Milano
P.za Leonardo da Vinci 32, 20133 Milan, IT.
guidotti@stru.polimi.it, csmerzini@stru.polimi.it

Keywords: Spectral Element Method; Discontinuous Galerkin; High Performance Computing; Seismic Wave Propagation; Earthquake Engineering.

AMS Subject Classification: 65M55, 65M70, 35Q86.

Abstract

This work presents a new high performance open-source numerical code, namely SPEED (*SP*ectral *E*lements in *E*lastodynamics with *D*iscontinuous *G*alerkin), to approach seismic wave propagation analysis in visco-elastic heterogeneous three-dimensional media on both local and regional scale. Based on non-conforming high-order techniques, like the Discontinuous Galerkin spectral approximation, along with efficient and scalable algorithms, the code allows one to deal with a non-uniform polynomial degree distribution as well as a locally varying mesh size. Validation benchmarks are illustrated to check the accuracy, stability and performance features of the parallel kernel, while illustrative examples are discussed to highlight the engineering applications of the method. The proposed method turns out to be particularly useful for a variety of earthquake engineering problems,

such as modeling of dynamic soil structure and site-city interaction effects, where accounting for multi-scale wave propagation phenomena as well as sharp discontinuities in mechanical properties of the media is crucial.

1 Introduction

Physics-based numerical modeling of the seismic response of arbitrarily complex earth media has gained major relevance in recent years, owing, on one side, to the ever-increasing progress in computational algorithms and resources, and, on the other side, to the growing interest towards the development of deterministic scenarios as input within seismic hazard and risk assessment studies. In the last twenty years there has been an impressive progress worldwide towards the development of high-order numerical methods for the simulation of seismic wave propagation under realistic tectonic and geo-morphological conditions. Such an advancement was boosted by several international benchmarks, regarding, for instance, the 3D seismic response of the Los Angeles basin (see e.g. [19]), of the Grenoble Valley (e.g. [12, 82]), and of the Euroseistest site (Cashima project, <https://www-cashima.cea.fr/>), as well as by innovative approaches to seismic hazard and risk assessment, such as in the CyberShake project (e.g. [33]) and in the Great Southern California ShakeOut Exercise (www.shakeout.org, e.g. [41, 7]). Furthermore, such a progress in numerical techniques has concerned not only forward but also inverse modelling, as attested by the growing number of applications in tomography of the Earth's interior as well as in seismic source inversion (e.g. [86, 68, 27]).

These examples testify the increasing need for certified numerical models apt to include the coupled effects of the seismic source, the propagation path through complex geological structures and localized superficial irregularities, such as alluvial basins or/and man-made infrastructures. However, accounting for all these features within a single model still poses challenging demands on computational methods and resources due to the coexistence of very different spatial scales, from a few tens of kilometers, with reference to the seismic fault, up to a few meters, or even less, when considering some structural elements. Motivated by these considerations, this work aims at developing a certified, flexible and highly accurate numerical software package for elastodynamics problems.

In the past twenty years, Spectral Element (SE) methods have emerged as one of the most effective and powerful approaches for solving three-dimensional seismic wave propagation problems in highly heterogeneous media (see, e.g., pioneering applications by [78, 25, 49]) owing to its capability of providing fast and highly accurate solutions along with its native orientation towards high performance parallel computing. The SE method, introduced firstly in fluid dynamics [67, 59], can be related to the N -version of the Finite Element (FE) method [5, 6]. The main idea behind SE method is that the finite dimensional space is made by high order (piecewise) interpolants, i.e., the Lagrangian polynomials, sampled at the Legendre-Gauss-Lobatto (LGL) quadrature points. This

discretization technique retains the geometrical flexibility of low-order finite elements while featuring the accuracy typical of spectral methods. Indeed, one of the key points of the SE method is the capability of providing an arbitrarily accurate numerical solution by simply enhancing the polynomial approximation degree [14]. Moreover, since it is based on the weak formulation of the elastodynamics equations, it naturally handles both interface continuity and free boundary conditions, ensuring the computation of accurate surface and interface waves.

Flexible numerical strategies in elastodynamics codes are nowadays mandatory due to i) the intrinsic multi-scale nature of seismic wave propagation problems, involving a relative broad range of wavelengths, ii) the complexity of the geometric constraints and iii) the difficulties of dealing with complex three dimensional heterogeneous media while keeping the computational effort low. For this reason, a non-conforming discretization approach, such as the Discontinuous Galerkin (DG) technique (see e.g. [3, 76, 38]), has been coupled with a SE method, in order to further improve its capabilities. In their general formulation, DGSE methods can deal with a nonuniform polynomial degree distribution (N -adaptivity), as well as a locally varying mesh size (h -adaptivity).

The DG method was first introduced by Reed and Hill [73] in 1973 for neutron transport equation. Since then, there has been a growing and active development of DG discretizations for a large set of problems, including parabolic and elliptic linear or non-linear partial differential equations [16]. The first application of DG technique to hyperbolic systems of equations come from the ninetens [26, 39, 28], while more recently, the analysis of the DG method has been extended to acoustic or elastic wave propagation, e.g. [13, 35, 63, 69, 74].

The first attempt to use the N -version of the DG approach for seismic wave propagation problems in heterogeneous media can be found in [42]. In this work the DG paradigm (in its flux formulation) is applied elementwise on conforming tetrahedral meshes and it is combined with the so-called Cauchy-Kovalewski approach to guarantee arbitrary high-order accuracy in both space and time variables. Nevertheless, the uncontrolled proliferation of degrees of freedom makes this approach computationally expensive: a local time stepping scheme is then needed to enhance the computational efficiency and the performance of the method [24].

A similar DG method is employed by [89] for the numerical solution of three-dimensional wave propagation problems in coupled elastic-acoustic media, using a velocity-strain formulation. In this work an explicit expression of the upwind numerical flux is derived as an exact solution for the relevant Riemann problem at elemental interfaces.

To overcome the drawbacks of the aforementioned approaches and to fully exploit the capabilities of the SE method, in the framework of a joint research activity between the Department of Structural Engineering and of Mathematics of Politecnico di Milano, an improved non-conforming formulation has been proposed and implemented in a new high performance open-source code, namely

SPEED (Spectral Elements in Elastodynamics with Discontinuous Galerkin: <http://mox.polimi.it/it/progetti/speed/SPEED/Home.html>). The code allows one to perform simulation of seismic wave propagation in visco-elastic heterogeneous three dimensional media, by exploiting non-conforming grids and/or variable approximation orders. With respect to the methods illustrated above, the one presented herein is employed only at a subdomain level, thus minimizing significantly the computational cost per element (see critical discussion in [22, 21, 20]). It is worth underlining that a similar approach has been already developed by [58, 57] for electromagnetic scattering problems. Nonetheless, in this work coupling between different discretizations is made through mortar interfaces, whereas in our study a DG approach is used for glueing together different subdomain discretizations. As it has been proven in [2], we recall herein that the proposed formulation is stable, provides optimal approximation properties, and yields low dispersion and dissipation errors.

In the first part of the paper we will focus on the model setting and the DGSE formulation is presented in order to clarify the mathematical model implemented in SPEED. In the second part a verification example will be illustrated to check the correctness and accuracy of the simulation scheme and, subsequently, to evaluate the performance features (efficiency and speed-up) of the parallel kernel. Finally, some application examples will be presented to shed light on the main advantages of the code and to testify its feasibility when dealing with challenging issues, such as modeling of Dynamic Soil-Structure and Site-City interaction effects. To the authors' knowledge, understanding and quantifying these effects in a fully coupled 3D numerical model is still at a research stage and has been addressed only by a few studies [40, 84, 56]. Furthermore, the applications, made possible by the improvements of the numerical scheme as well as of the performance features of the code, represent a step further in promoting a novel "from-the-seismic-source-to-the-structure" multi-scale computing approach for seismic risk assessment.

2 Model problem and governing equations

In this section the fundamental equations of elastodynamics, as implemented in SPEED, are described with emphasis on the non-conforming paradigm. For further details, the reader is referred to [2]. Let us consider an elastic heterogeneous medium occupying an open, bounded region $\Omega \subset \mathbb{R}^3$, with Lipschitz boundary $\Gamma := \partial\Omega$.

The boundary consists of the portions Γ_D , where the displacement vector \mathbf{u} is prescribed, Γ_N where external surface loads \mathbf{p} apply, and Γ_{NR} where suitable non-reflecting boundary conditions are imposed (see e.g., [80]). We suppose that Γ_D , Γ_N and Γ_{NR} are disjoint, i.e. $\Gamma_D \cap \Gamma_N = \emptyset$ and $\Gamma_N \cap \Gamma_{NR} = \emptyset$ and either Γ_N or Γ_{NR} can be empty.

For a given displacement vector \mathbf{v} , let $\boldsymbol{\sigma}(\mathbf{v})$ be the Cauchy stress tensor

$$\boldsymbol{\sigma}(\mathbf{v}) := \lambda(\nabla \cdot \mathbf{v})\mathbf{I} + 2\mu\boldsymbol{\varepsilon}(\mathbf{v}),$$

where $\boldsymbol{\varepsilon}(\mathbf{v}) := 1/2(\nabla\mathbf{v} + \nabla\mathbf{v}^\top)$ is the strain tensor, \mathbf{I} is the identity tensor and λ, μ are the Lamè parameters. For a given density of body forces \mathbf{f} , and a given vector field \mathbf{p} , we consider the linear elastodynamics system:

$$\rho\mathbf{u}_{tt} - \nabla \cdot \boldsymbol{\sigma}(\mathbf{u}) = \mathbf{f}, \quad \text{in } \Omega \times (0, T], \quad (1)$$

coupled with boundary conditions

$$\mathbf{u} = \mathbf{0} \quad \text{on } \Gamma_D, \quad \boldsymbol{\sigma}(\mathbf{u})\mathbf{n} = \mathbf{p}^* \quad \text{on } \Gamma_N \cup \Gamma_{NR}, \quad (2)$$

where \mathbf{n} is the unit outward normal vector to Γ and $\mathbf{p}^* := \mathbf{p}$ on Γ_N and

$$\mathbf{p}^* := \rho(V_P - V_S)(\mathbf{u}_t \cdot \mathbf{n})\mathbf{n} + \rho V_S \mathbf{u}_t \quad \text{on } \Gamma_{NR}. \quad (3)$$

Here, $V_P := \sqrt{(\lambda + 2\mu)/\rho}$ and $V_S := \sqrt{\mu/\rho}$ are the propagation velocities of P and S waves, respectively. At the artificial model boundary Γ_{NR} , waves travelling out of the domain Ω need to be absorbed. However, the representation of this (radiation) condition associated with the external boundaries is a delicate issue, since, ideally, such boundaries should be able to propagate any incident wave without reflections. In literature numerous numerical schemes have been proposed (e.g., [29]). Here, we adopt a first order approximation (3) close to the one proposed by Stacey [80] that is based upon a one-way treatment that perfectly absorbs waves impinging at right angles to the boundary, but that is less effective for waves that graze the boundary [15]. It should be mentioned that the implementation in the code of more recent and efficient absorbing boundary conditions, such as the Convolution Perfectly Matched Layer (CPML), is expected to provide some improvements. As a matter of fact, CPMLs perform much better than the paraxial conditions and can attenuate surface waves as well as body waves with grazing incidence (for details see [60]).

Finally, to complete the system (1)–(3) we prescribe initial conditions $\mathbf{u} = \mathbf{u}_0$ and $\mathbf{u}_t = \mathbf{u}_1$ for the displacement and the velocity field, respectively. We remark that for heterogeneous media, ρ, λ and μ are bounded functions of the spatial variable, not necessarily continuous, i.e., ρ, λ and $\mu \in L^\infty(\Omega)$.

The main difficulty in the incorporation of visco-elasticity within time marching codes relies in the implementation of a convolution process between stress and strain, as required by a straightforward application of visco-elastic models in the time domain. As an alternative, approximate techniques for modelling visco-elastic media within the framework of discrete grid time domain schemes have been proposed making use of a suitable modification of the equation of motion, see e.g. [31]. This is the approach used in SPEED to account for spatially varying visco-elastic materials, characterized by a suitable decay factor ξ [s^{-1}],

defined in the sequel. The governing equation (1) is then modified by introducing two equivalent volume forces, leading to the following expression:

$$\rho \mathbf{u}_{tt} + 2\rho\xi \mathbf{u}_t + \rho\xi^2 \mathbf{u} - \nabla \cdot \boldsymbol{\sigma}(\mathbf{u}) = \mathbf{f}, \quad \text{in } \Omega \times (0, T]. \quad (4)$$

It can be shown [53] that, with such replacement, all frequency components are equally attenuated, resulting in a frequency proportional quality factor

$$Q = Q_0 \frac{f}{f_0},$$

where $Q_0 = \pi f_0 / \xi$, with ξ being the decay factor and f_0 a reference value representative of the frequency range to be propagated.

Here and in the sequel we use the standard notation [1] to define the L^2 -inner product for scalar, vector and tensor quantities, and the direct product of the functional space X by itself will be denoted by \mathbf{X} .

3 Discontinuous Galerkin spectral element discretization

In this section we introduce the discontinuous Galerkin spectral formulation for the problem (1)–(2). The non-conforming paradigm will be applied as in [2] at a first (subdomain) level as explained in the sequel. For the sake of simplicity we suppose $\Gamma := \Gamma_D \cup \Gamma_N$. For the general case in which both viscous forces (4) and absorbing boundary conditions (3) apply, we refer the reader to [61].

3.1 Non-conforming domain partitioning

The discretization approach as implemented in SPEED can be described as a three-levels process.

1 Level. On a first level, the domain Ω is partitioned into R non-overlapping polygonal subdomains, i.e. $\Omega = \bigcup_{j=1}^R \Omega_j$, with sufficiently smooth boundary $\Gamma_j := \partial\Omega_j$. This decomposition can be geometrically non-conforming, i.e., for two adjacent subdomains Ω_k, Ω_i , the surface $\Lambda := \Gamma_k \cap \Gamma_i$ may not be a complete side of either Ω_k or Ω_i (see Figure 1).

2 Level. On a second level, for each Ω_k we define a conforming partition \mathcal{T}_k , such that $\Omega_k = \bigcup_{j=1}^{R_k} \Omega_k^j$. The elements Ω_k^j have typical linear size h_k , ($h_k = \max_j h_k^j$, with $h_k^j = \text{diam}(\Omega_k^j)$) and are obtained by mapping the reference cube $\Omega^* = (-1, 1)^3$ with a suitable bilinear map $\mathbf{F}_k^j : \Omega^* \rightarrow \Omega_k^j$ with non-zero Jacobian \mathbf{J}_k^j . The global partition is then obtained as $\mathcal{T} = \bigcup_{j=1}^R \mathcal{T}_j$ and must preserve the boundary decomposition introduced in (2). This second-level partition is geometrically conforming in each Ω_k , thus the intersection of two

elements $\Omega_k^j, \Omega_k^i \in \Omega_k$ for $j \neq i$, is either empty, or a vertex, or an edge, or a face of both Ω_k^j and Ω_k^i .

3 Level. The third level is represented by the so-called Legendre-Gauss-Lobatto (LGL) points \mathbf{x}_i in each mesh element Ω_k^i , see Figure 1. On the reference element Ω^* , these points are defined as the tensor product of LGL points defined in the interval $[-1, 1]$, see [71]. Then, they are mapped on the physical element Ω_k^i by \mathbf{F}_k^i .

Based on the aforementioned domain discretization we introduce in each Ω_i^j the space

$$\mathbf{Q}_{N_i}(\Omega_i^j) := \{\mathbf{v} = \mathbf{v}^* \circ (\mathbf{F}_i^j)^{-1} : \mathbf{v}^* \in \mathbf{Q}_{N_i}(\Omega^*)\},$$

where $\mathbf{Q}_{N_i}(\Omega^*)$ is the space of vectorial functions defined over Ω^* and such that each component is an algebraic polynomial of degree less than or equal to $N_i \geq 1$ in each space variable. We define the finite dimensional spaces

$$\mathbf{X}(\Omega_i) := \{\mathbf{v} \in \mathbf{C}^0(\overline{\Omega}_i) : \mathbf{v}|_{\Omega_i^j} \in \mathbf{Q}_{N_i}(\Omega_i^j), \forall \Omega_i^j \in \mathcal{T}_i\},$$

and, finally,

$$\mathbf{V}_\delta(\Omega) := \{\mathbf{v}_\delta \in \mathbf{L}^2(\Omega) : \mathbf{v}_\delta|_{\Omega_i} \in \mathbf{X}(\Omega_i), i = 1, \dots, R : \mathbf{v}_\delta|_{\Gamma_D} = \mathbf{0}\},$$

where $\delta := \{\mathbf{h}, \mathbf{N}\}$ with $\mathbf{h} := (h_1, \dots, h_R)$ and $\mathbf{N} := (N_1, \dots, N_R)$ are couplets of discretization parameters. Each component h_i and N_i represents the mesh size and the degree of the polynomial interpolation in the region Ω_i , respectively.

A nodal basis for \mathbf{V}_δ is obtained introducing on each element Ω_i^j the LGL points and the corresponding degrees of freedom which allow to identify uniquely a generic function in \mathbf{V}_δ . In the spectral element approach the interpolation LGL-points are used also as quadrature points; thus, we have

$$(f, g)_{\Omega_i^j} \approx (f, g)_{NI, \Omega_i^j} := \sum_{k=1}^{(N_i+1)^3} (f \circ \mathbf{F}_i^j)(\mathbf{x}_k) \cdot (g \circ \mathbf{F}_i^j)(\mathbf{x}_k) |det(\mathbf{J}_i^j)| \omega_k, \quad (5)$$

where ω_k are the weights of the LGL quadrature formula [14] an NI stands for numerical integration. The spectral shape functions $\Phi_i \in \mathbf{V}_\delta$ are defined such that $\Phi_i(\mathbf{x}_j) = \delta_{ij}$, $i, j = 1, \dots, (N_i + 1)^3$, where δ_{ij} is the Kronecker symbol.

It is straightforward to see that by the definition of \mathbf{V}_δ , the basis functions will not be globally continuous on the whole domain and that the restriction of any spectral function to Ω_i^j either coincides with a Lagrange polynomial or vanishes. Moreover, the support of any shape function is limited to the neighbouring elements if the spectral node lies on the interface between two or more elements, while it is limited to only one element for internal nodes.

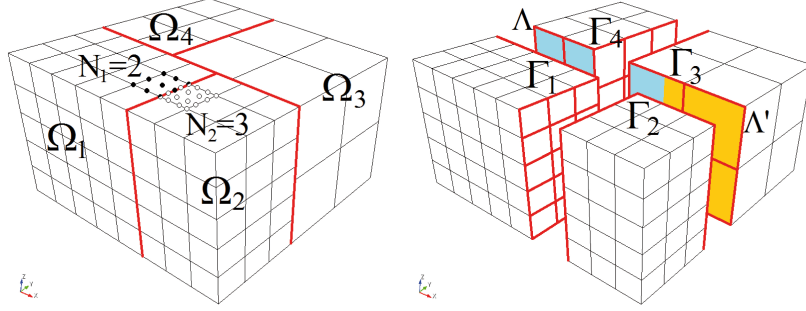


Figure 1: 3D example of non-conforming domain decomposition. The whole domain is composed by different non-overlapping polygonal subdomains, made by hexahedral elements. Highlighted are the boundary surfaces between different subdomains. DG discretization allows to deal with a non-uniform polynomial degree distribution (\mathbf{N} -adaptivity, e.g., $N_1 = 2$ in Ω_1 and $N_2 = 3$ in Ω_2), as well as a locally varying mesh size (\mathbf{h} -adaptivity between sub-domains $\Omega_1, \Omega_2, \Omega_3$ and Ω_4). The surface between two neighbouring sub-domains Ω_k and Ω_i , then may not be a complete side of Ω_k or Ω_i (e.g. Λ and Λ').

3.2 Discontinuous Galerkin weak formulation

In this section we present the variational formulation for the problem (1)–(2) obtained using the Discontinuous Galerkin spectral element discretization described in the previous paragraph.

We start defining an interior face as the non-empty interior of the intersection of two neighbouring elements belonging to different subdomains. More precisely, let $\Omega_k^i \in \Omega_k$ and $\Omega_m^j \in \Omega_m$ be two neighbouring elements, we set $\bar{\gamma}_\ell := \partial\bar{\Omega}_k^i \cap \partial\bar{\Omega}_m^j$, where $\ell := \ell(i, j, k, m)$. We express the skeleton \mathcal{S} of the domain Ω as the union of elementary components γ_ℓ , more precisely, $\bar{\mathcal{S}} := \bigcup_{\ell=1}^M \bar{\gamma}_\ell$, for some positive integer M . We remark that this decomposition is unique. For any pair of adjacent elements Ω_k^i and Ω_m^j sharing a non-trivial edge γ , we denote by $\mathbf{v}^i, \boldsymbol{\sigma}^i$ (resp. $\mathbf{v}^j, \boldsymbol{\sigma}^j$) the restriction to Ω_k^i (resp. Ω_m^j) of regular enough functions $\mathbf{v}, \boldsymbol{\sigma}$. We also denote by \mathbf{n}^i (resp. \mathbf{n}^j) the exterior unit normal to Ω_k^i (resp. Ω_m^j). On each γ we define the average and jump operators for \mathbf{v} , and $\boldsymbol{\sigma}$ as follows:

$$\{\mathbf{v}\} := \frac{1}{2}(\mathbf{v}^i + \mathbf{v}^j), \quad \llbracket \mathbf{v} \rrbracket := \mathbf{v}^i \otimes \mathbf{n}^i + \mathbf{v}^j \otimes \mathbf{n}^j, \quad (6)$$

and

$$\{\boldsymbol{\sigma}\} := \frac{1}{2}(\boldsymbol{\sigma}^i + \boldsymbol{\sigma}^j), \quad \llbracket \boldsymbol{\sigma} \rrbracket := \boldsymbol{\sigma}^i \mathbf{n}^i + \boldsymbol{\sigma}^j \mathbf{n}^j, \quad (7)$$

where $\mathbf{a} \otimes \mathbf{b} \in \mathbb{R}^{3 \times 3}$ is the tensor with entries $(\mathbf{a} \otimes \mathbf{b})_{ij} := a_i b_j, 1 \leq i, j \leq 3$, for all $\mathbf{a}, \mathbf{b} \in \mathbb{R}^3$. After multiplication of (1) by a test function $\mathbf{v} \in \mathbf{V}_\delta$, integration

by parts over each Ω_j , for $j = 1, \dots, R$, and using that

$$\sum_{k=1}^R (\boldsymbol{\sigma}(\mathbf{u})\mathbf{n}, \mathbf{v})_{\partial\Omega_k \setminus \partial\Omega} = \sum_{\ell=1}^M (\{\boldsymbol{\sigma}(\mathbf{u})\}, \llbracket \mathbf{v} \rrbracket)_{\gamma_\ell} + (\llbracket \boldsymbol{\sigma}(\mathbf{u}) \rrbracket, \{\mathbf{v}\})_{\gamma_\ell},$$

we deduce that:

$$(\rho \mathbf{u}_{tt}, \mathbf{v})_\Omega + (\boldsymbol{\sigma}(\mathbf{u}), \boldsymbol{\varepsilon}(\mathbf{v}))_\Omega - (\{\boldsymbol{\sigma}(\mathbf{u})\}, \llbracket \mathbf{v} \rrbracket)_\mathcal{S} - (\llbracket \boldsymbol{\sigma}(\mathbf{u}) \rrbracket, \{\mathbf{v}\})_\mathcal{S} = (\mathbf{f}, \mathbf{v})_\Omega + (\mathbf{p}, \mathbf{v})_{\Gamma_N}.$$

Now, imposing the continuity of tractions across \mathcal{S} , i.e. $\llbracket \boldsymbol{\sigma} \rrbracket = \mathbf{0}$, yields to:

$$(\rho \mathbf{u}_{tt}, \mathbf{v})_\Omega + (\boldsymbol{\sigma}(\mathbf{u}), \boldsymbol{\varepsilon}(\mathbf{v}))_\Omega - (\{\boldsymbol{\sigma}(\mathbf{u})\}, \llbracket \mathbf{v} \rrbracket)_\mathcal{S} = (\mathbf{f}, \mathbf{v})_\Omega + (\mathbf{p}, \mathbf{v})_{\Gamma_N}. \quad (8)$$

Since also $\llbracket \mathbf{u} \rrbracket = 0$ across the boundary, we can add further terms in (8) that penalize and control the jumps of the numerical solution across \mathcal{S} , such as:

$$- (\llbracket \mathbf{u}_\delta \rrbracket, \{\boldsymbol{\sigma}(\mathbf{v})\})_\mathcal{S} + \sum_{\ell=1}^M \eta_\ell (\llbracket \mathbf{u}_\delta \rrbracket, \llbracket \mathbf{v} \rrbracket)_{\gamma_\ell}, \quad (9)$$

where η_ℓ are positive constants depending on the discretization parameters \mathbf{h} and \mathbf{N} and on the Lamé coefficients. The terms in (9) do not affect consistency of the method and are added with the purpose of providing more generality and better stability properties to the scheme (see [76, 74]). Hereinafter we set

$$\eta_\ell := \alpha \{\lambda + 2\mu\}_A \mathbf{h}_\ell / \mathbf{N}_\ell^2 \quad (10)$$

where α is a positive constant at disposal, $\{q\}_A$ is the harmonic average of the quantity q and $\mathbf{N}_\ell := \max(N_k, N_m)$, $\mathbf{h}_\ell := \text{area}(\gamma_\ell)$ if $\gamma_\ell = \partial\Omega_k^i \cap \partial\Omega_m^j$.

Then, the semi-discrete DG formulation reads: for all $t \in (0, T]$ find $\mathbf{u}_\delta := \mathbf{u}_\delta(t) \in \mathbf{V}_\delta$ such that:

$$(\rho \partial_{tt} \mathbf{u}_\delta, \mathbf{v})_\Omega + \mathcal{A}(\mathbf{u}_\delta, \mathbf{v})_\Omega = (\mathbf{f}, \mathbf{v})_\Omega + (\mathbf{p}, \mathbf{v})_{\Gamma_N} \quad \forall \mathbf{v} \in \mathbf{V}_\delta, \quad (11)$$

where

$$\begin{aligned} \mathcal{A}(\mathbf{u}, \mathbf{v})_\Omega &= \sum_{k=1}^R (\boldsymbol{\sigma}(\mathbf{u}), \boldsymbol{\varepsilon}(\mathbf{v}))_{\Omega_k} + \sum_{\ell=1}^M \left[\eta_{\gamma_\ell} (\llbracket \mathbf{u} \rrbracket, \llbracket \mathbf{v} \rrbracket)_{\gamma_\ell} \right. \\ &\quad \left. - (\{\boldsymbol{\sigma}(\mathbf{u})\}, \llbracket \mathbf{v} \rrbracket)_{\gamma_\ell} - (\llbracket \mathbf{u} \rrbracket, \{\boldsymbol{\sigma}(\mathbf{v})\})_{\gamma_\ell} \right]. \end{aligned} \quad (12)$$

Equation (11) corresponds to the symmetric interior penalty Galerkin (SIPG) method [3]. Other formulations (e.g., non-symmetric or incomplete) can be obtained similarly (see [3, 76, 74, 75] for more details). We remark that problem (11) is well posed and admits a unique solution $\mathbf{u}_\delta \in \mathbf{H}^2((0, T], \mathbf{V}_\delta)$ provided that the bilinear form $\mathcal{A}(\cdot, \cdot)$ is continuous and coercive with respect a suitable energy norm. Moreover the discrete solution \mathbf{u}_δ satisfies optimal error estimate with respect to the mesh size, see [2] for more details.

3.3 Algebraic formulation and time integration scheme

The description of the discretization technique is completed by the discussion of the algebraic formulation of (11) and by the introduction of the time integration scheme adopted in SPEED.

We start by introducing a basis $\{\Phi_i^1, \Phi_i^2, \Phi_i^3\}_{i=1}^D$, for the finite dimensional space \mathbf{V}_δ , where D represents the degrees of freedom of the problem and $\Phi_i^1 := (\Phi_i, 0, 0)^\top$, $\Phi_i^2 := (0, \Phi_i, 0)^\top$ and $\Phi_i^3 := (0, 0, \Phi_i)^\top$. Omitting the subscript δ , we write the discrete function $\mathbf{u} \in \mathbf{V}_\delta$ as

$$\mathbf{u}(\mathbf{x}, t) := \sum_{j=1}^D \Phi_j^1(\mathbf{x})U_j^1(t) + \Phi_j^2(\mathbf{x})U_j^2(t) + \Phi_j^3(\mathbf{x})U_j^3(t).$$

Then, using the above expression, we recast equation (11) for any test function $\Phi_i^\ell(\mathbf{x}) \in \mathbf{V}_\delta$, for $\ell = 1, \dots, 3$, obtaining the following set of discrete ordinary differential equations for the nodal displacement $\mathbf{U} := [\mathbf{U}^1, \mathbf{U}^2, \mathbf{U}^3]^\top$;

$$M\ddot{\mathbf{U}} + A\mathbf{U} = \mathbf{F}, \quad (13)$$

where $\ddot{\mathbf{U}}$ represents the vector of nodal acceleration and \mathbf{F} the vector of externally applied loads:

$$\mathbf{F} := [\mathbf{F}^1, \mathbf{F}^2, \mathbf{F}^3]^\top, \quad \mathbf{F}_i^\ell := (\mathbf{f}, \Phi_i^\ell)_{NI, \Omega} + (\mathbf{p}, \Phi_i^\ell)_{NI, \Gamma_N}, \quad \text{for } i = 1, \dots, D.$$

Rewriting equation (13) component-wise we have that

$$\begin{bmatrix} M^1 & 0 & 0 \\ 0 & M^2 & 0 \\ 0 & 0 & M^3 \end{bmatrix} \begin{bmatrix} \ddot{\mathbf{U}}^1 \\ \ddot{\mathbf{U}}^2 \\ \ddot{\mathbf{U}}^3 \end{bmatrix} + \begin{bmatrix} A^{11} & A^{12} & A^{13} \\ A^{21} & A^{22} & A^{23} \\ A^{31} & A^{32} & A^{33} \end{bmatrix} \begin{bmatrix} \mathbf{U}^1 \\ \mathbf{U}^2 \\ \mathbf{U}^3 \end{bmatrix} = \begin{bmatrix} \mathbf{F}^1 \\ \mathbf{F}^2 \\ \mathbf{F}^3 \end{bmatrix},$$

and as a consequence of assumptions on the basis functions given in section 3.1, and by means of (5) we have that the mass matrix M has a diagonal structure with elements

$$M_{ij}^\ell := (\rho \Phi_j^\ell, \Phi_i^\ell)_{NI, \Omega} \quad \text{for } i, j = 1, \dots, D, \text{ and } \ell = 1, \dots, 3,$$

while the matrix A associated to the bilinear form $\mathcal{A}(\cdot, \cdot)$ defined in (12) is such that for $i, j = 1, \dots, D$ it holds

$$A_{ij}^{\ell k} := \mathcal{A}(\Phi_j^\ell, \Phi_i^k)_{NI, \Omega} \quad \text{for } k, \ell = 1, \dots, 3.$$

Now, we define $\mathbf{V} := \dot{\mathbf{U}}$ the vector of nodal velocities, we prescribe initial conditions $\mathbf{U}(0) = \mathbf{u}_0$ and $\mathbf{V}(0) = \mathbf{u}_1$ and we consider the system (13). Let us now subdivide the interval $(0, T]$ into N subintervals of amplitude $\Delta t = T/N$ and set $t_n = n\Delta t$, for $n = 1, \dots, N$.

The Newmark method, see e.g. [72], applied to (13) consists in finding the approximations $\{\mathbf{U}(t_n)\}_n$ to $\mathbf{u}(t_n)$ such that for $n \geq 2$,

$$\begin{aligned} [M + \Delta t^2 \beta A] \mathbf{U}(t_{n+1}) &= \left[2M - \Delta t^2 \left(\frac{1}{2} - 2\beta + \vartheta \right) A \right] \mathbf{U}(t_n) \\ &\quad - [M + \Delta t^2 \left(\frac{1}{2} + \beta - \vartheta \right)] \mathbf{U}(t_{n-1}) \\ &\quad + \Delta t^2 [\beta \mathbf{F}(t_{n+1}) + \left(\frac{1}{2} - 2\beta + \vartheta \right) \mathbf{F}(t_n) + \left(\frac{1}{2} + \beta - \vartheta \right) \mathbf{F}(t_{n-1})], \end{aligned} \quad (14)$$

with

$$\begin{aligned} [M + \Delta t^2 \beta A] \mathbf{U}(t_1) &= \left[M - \Delta t^2 \left(\frac{1}{2} - \beta \right) A \right] \mathbf{U}(t_0) \\ &\quad - \Delta t M \mathbf{V}(t_0) + \Delta t^2 [\beta \mathbf{F}(t_1) + \left(\frac{1}{2} - \beta \right) \mathbf{F}(t_0)]. \end{aligned} \quad (15)$$

Notice that, at each time step t_{n+1} the solution of (15) can be obtained provided $\mathbf{U}(t_n)$ and $\mathbf{U}(t_{n-1})$ are known. Here, $\beta \geq 0$ and $\vartheta \geq \frac{1}{2}$ are parameters to be chosen. We recall that for $\vartheta = \frac{1}{2}$ the Newmark scheme is second order accurate in time, whereas it is only first order accurate for $\vartheta > \frac{1}{2}$. For $\beta = 0$ the Newmark scheme (15)-(14) requires at each time step the solution of a linear system with the mass matrix M . However because M is diagonal it can be inverted at very low computational cost and the scheme is essentially fully explicit. With $\vartheta = \frac{1}{2}$, the explicit Newmark method corresponds to the standard leap-frog scheme

$$M \mathbf{U}(t_{n+1}) = [2M - \Delta t^2 A] \mathbf{U}(t_n) - M \mathbf{U}(t_{n-1}) + \Delta t^2 \mathbf{F}(t_n), \quad (16)$$

for $n = 1, \dots, N$, with

$$M \mathbf{U}(t_1) = \left[M - \frac{\Delta t^2}{2} A \right] \mathbf{U}(t_0) - \Delta t M \mathbf{V}(t_0) + \frac{\Delta t^2}{2} \mathbf{F}(t_0).$$

We remark that the above scheme is stable if the time step Δt satisfies a Courant-Friedrichs-Lewy (CFL) condition $\Delta t \leq C_{CFL} \Delta x / V_P$, where Δx is the shortest distance between two LGL nodes and C_{CFL} is a constant depending on the dimension, the order of the scheme, the mesh geometry and the polynomial degree. Since $\Delta x \approx N^{-2}$ (see [14]) it follows that $C_{CFL} \approx N^{-2}$. The grid dispersion and dissipation properties of the leap-frog method coupled with DG discretization has been analysed in [2, 61], in particular it is shown that, heuristically, 5 points per wavelength are sufficient for providing negligible errors (less than 10^{-6}). This makes the proposed scheme well suited for the approximation of wave propagation problems as we are going to show in the next section.

4 Engineering problems of seismic wave propagation through the Discontinuous Galerkin approach

Non-conforming approaches, as the one described in the previous chapter, turn out to be particularly useful in engineering problems of seismic wave propagation, whenever complex geometries or sharp discontinuities of mechanical properties of the media are to be accounted for. As a matter of fact, the computational burden necessary to encompass within a single numerical model the intrinsic multi-scale nature of seismic wave propagation problems, from the far-field to the near-field and from the near-field to the soil-structure and site-city interaction effects, with characteristic size of the elements varying from several kilometers to few meters, has long limited the development of proper computational models.

The aim of this section is two-fold. On one side, verification tests, for both conforming and non-conforming meshes, are illustrated to check the correctness and accuracy of the code. Furthermore, additional tests were performed to examine the performance features, i.e., efficiency and speed-up, of the parallel kernel. On the other hand, some challenging applications are presented to highlight the main features of the code and its capabilities in tackling a variety of seismic engineering problems.

In particular, two case studies are shown: first, the simulation of a dynamic soil-structure interaction problem, with reference to the Acquasanta railway viaduct, located in the neighbourhood of Genoa, NW Italy; second, the study of site-city interaction effects in the Central Business District of Christchurch, during the destructive 22 February 2011 M_W 6.3 earthquake. Both applications were selected as representative benchmarks owing to the complexity of the mesh generation and to the coexistence of very different spatial scales that characterize the fully coupled dynamic problem.

The numerical models shown in the next sections have been created using the commercial software CUBIT (<http://cubit.sandia.gov/>), that features a set of advanced meshing algorithms suitable for handling 3D unstructured hexahedral decomposition. Nonetheless, SPEED has been designed to handle any hexahedral meshes, independently from the specific mesh generator. The resulting models usually reach a global number of several millions of degrees of freedom, requiring a huge level of parallelization, so that the simulations need to be performed at High-Performance Computing (HPC) Centers. Here, the Lagrange cluster located at the HPC Center CINECA-CILEA (<http://www.cilea.it/1/>) was used to perform the numerical simulations shown in this work. We remark that the parallel kernel of SPEED, in the version presented here, is based upon the MPI paradigm for managing communications between single processors, while recent improvements of the code have led to a hybrid OpenMP-MPI programming for boosting the performances. This latter release has been optimized on the Fermi cluster at CINECA computing centre (<http://www.cineca.it/en>). It is worth noting that in recent years there has been an increasing interest of the HPC

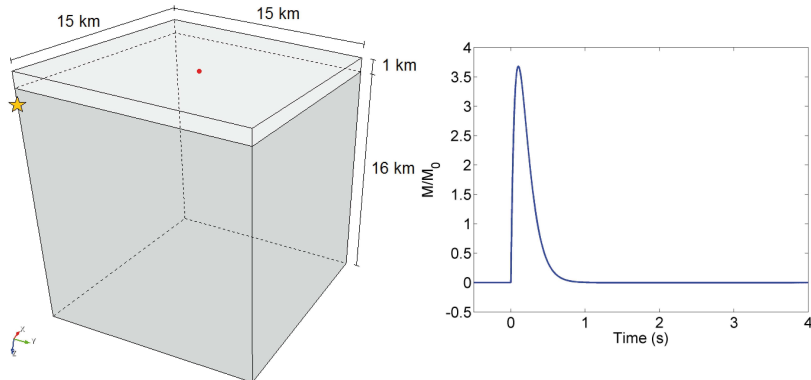


Figure 2: Left hand side: LOH Benchmark test, only one of the four symmetric quadrants is shown, the source (yellow star) is located at 2 km depth and different colors mean different mechanical characteristics; in red the receiver considered. Right hand side: moment rate function for the validation-test.

Table 1: Dynamic and mechanical parameters for the layer (L) and the halfspace (HS) of the LOH test.

Layer	Depth [m]	V_p [m/s]	V_S [m/s]	ρ [Kg/m ³]
L	0-1000	4000	2000	2600
HS	1000-17000	6000	3464	2700

community towards graphic card computing (GPU) not only as a viable architecture for general purpose computations but also as high performance approach for massive parallel computations. Moreover, this programming paradigm has been applied successfully for simulating seismic wave propagation (see e.g. [45, 46, 47] and references therein for further details).

4.1 Verification, efficiency and speed up

As a verification test of SPEED, the benchmark [18] was considered. The problem, depicted in Figure 2, is known in literature with the acronym LOH (Layer Over Halfspace) and it is currently a reference benchmark for different advanced numerical codes for seismic wave propagation (see e.g., [43, 82]). The computational domain is $\Omega = [(-15, 15) \times (-15, 15) \times (17, 0)]$ km, with the top layer having thickness 1 km. The characteristics of the materials are synthesized in Table 1.

The seismic source (see [25] for implementation issues) is given by a point double couple located at the center of the model:

$$\mathbf{f}(\mathbf{x}) = \nabla \delta(\mathbf{x} - \mathbf{x}_S) M(t), \quad (17)$$

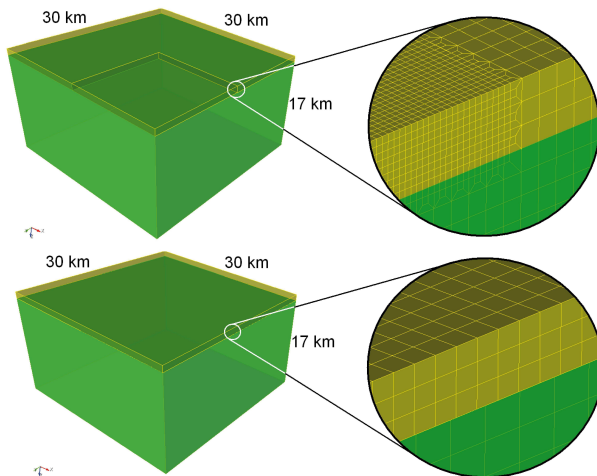


Figure 3: LOH conforming model, having size of $30 \times 30 \times 17 \text{ km}$: (Top) conforming mesh with 814.833 hexahedral elements, varying from size of 100 m , in the first quadrant, to 300 m in the remaining part of the domain; (Bottom) non-conforming model with 70.228 hexahedral elements, having size of around 400 m in the upper layer (1 km thickness) and size of around 650 m in the lower layer (16 km thickness).

Table 2: Main characteristics of the conforming and non-conforming numerical models for the LOH test, with the main parameters of the analysis performed at Lagrange cluster, located at CILEA.

Mesh	Elements	\mathbf{N}	LGL nodes	Δt	Cores	Set up [h]	Total time [h]
Conforming	814833	4	$52.6 \cdot 10^6$	$3 \cdot 10^{-4}$ (20% CFL)	128	≈ 0.42	≈ 3.04
Non-conforming	70228	5	$9.0 \cdot 10^6$	$5 \cdot 10^{-4}$ (7% CFL)	128	≈ 0.58	≈ 3.53

where $\mathbf{x}_S = (0, 0, 2) \text{ km}$. The moment rate time variation $M(t)$, shown in Figure 2, is given by the following expression:

$$M(t) = M_0(t/t_0^2) \exp(-t/t_0), \quad (18)$$

where M_0 is the scalar seismic moment, equal to 10^8 Nm , t_0 is the “smoothness” parameter, controlling the frequency content and amplitude of the source time function, and $t_0 = 0.1 \text{ s}$. Further details on the problem setting as well as on the source time function can be found in [18], together with the expression of the semi-analytic solution. In this case two different models were considered and implemented in SPEED, the first one relying on a conforming spectral element discretization (Figure 3 top) and the second one using the DGSE approach described earlier (Figure 3 bottom). The characteristics of the numerical models and the main parameters of the analysis are listed in Table 2.

We report in Figure 4 the velocity wave field recorded at point $(6, 8, 0)$ km (see Figure 2) on the top layer along with the reference solution (see [18]). In each plot, we also report the relative seismogram misfit:

$$E = \frac{\sum_{i=1}^{n_s} (\mathbf{u}_\delta(t_i) - \mathbf{u}(t_i))^2}{\sum_{i=1}^{n_s} \mathbf{u}(t_i)^2} \quad (19)$$

where n_s is the number of time samples of the seismogram, $\mathbf{u}_\delta(t_i)$ is the numerical value of the seismogram at sample t_i , and $\mathbf{u}(t_i)$ is the corresponding reference value. The maximum relative misfit with respect to the reference solution is less than 1% for the conforming model and around 2% for the non-conforming one. It is important to underline that the non conforming model has a sensibly lower number of elements, nonetheless the accuracy of the solution is preserved (see Figure 4). These results are promising, especially compared to those available in literature (see e.g., [82, 43]). Further improvements of the results can be achieved, for instance, choosing higher order polynomial degrees.

With reference to the two different models, represented in Figure 3, several tests have been performed on the Lagrange cluster, by varying the number of cores adopted for the computation, to evaluate the performance of the parallel algorithm, in terms of efficiency and speed-up. The results, as histograms, are plotted in Figure 5 against the ideal behaviour, considering the total computing time.

The behaviour of the parallel kernel with 32 cores has been taken as the reference solution, therefore, in this case, both efficiency and speed-up values are equal to the ideal case. The efficiency and speed-up as a function of the number of cores, varying from 64 to 512, point out the good performances of SPEED. For instance, considering 512 cores, the efficiency is around 90% and 70% of the ideal efficiency for the conforming and non-conforming model, respectively. A similar performance can be observed also in terms of speed-up.

4.2 The Acquasanta Railway Bridge

As a first engineering application, a soil-structure interaction problem, concerning the seismic response of the Acquasanta bridge, located on the Genoa-Ovada railway, NW Italy, in the Genoa district, is considered. The structure is a typical arch-bridge and it is remarkable both for the site features and the local geological and geomorphological conditions. The foundations of several piers, indeed, rest on weak rock and, moreover, some instability problems have been detected in the past on the valley slope westward, towards Ovada, [79]. A detailed description of the structural characteristics of the bridge as well as of the geological setting (see Table 3) can be found in [81]. A 3D numerical model was created encompassing both the seismic source, the surrounding geological model and the Acquasanta bridge.

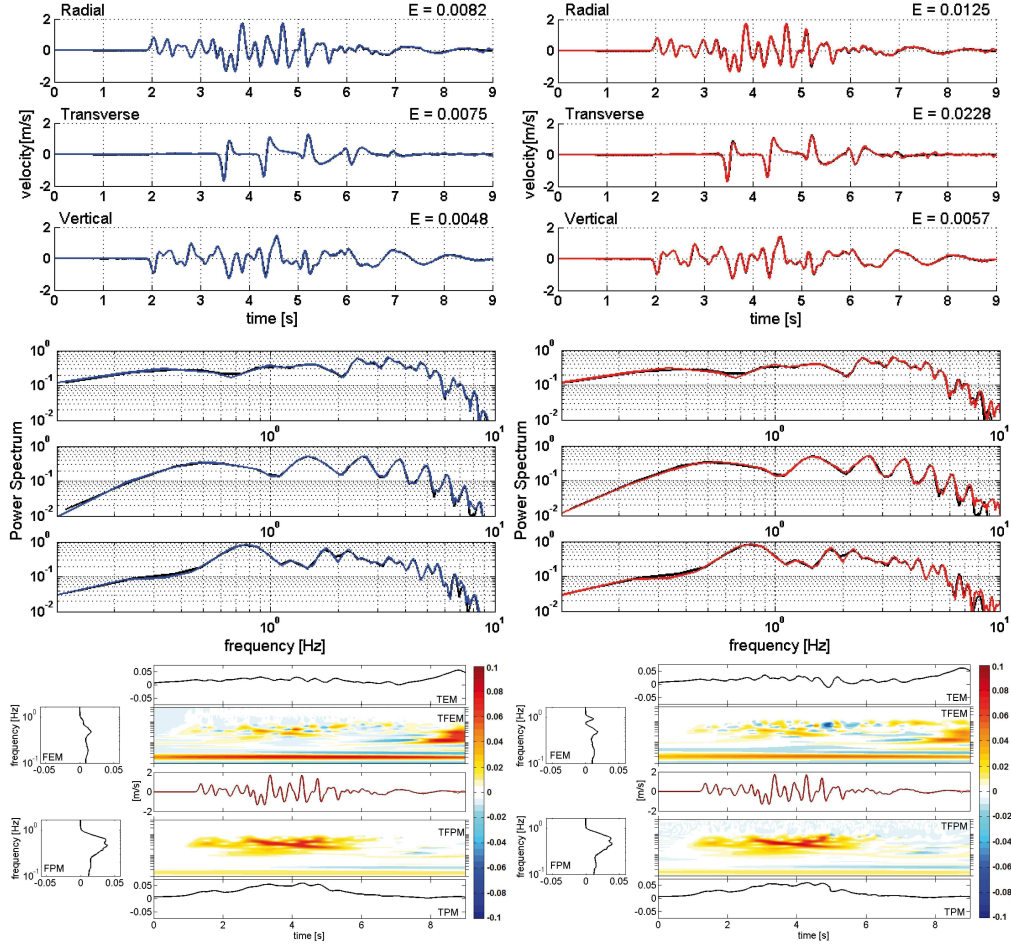


Figure 4: Velocity field recorded at $(6,8,0)$ km . Comparison in the Time and Frequency domain between the semi-analytic solution (black line) and the numerical one (coloured line). Relative misfit computed according with equation (19) and, for the signal along x axis, with [54], (FEM : Frequency-dependent envelope misfit; TEM : Time-dependent envelope misfit; $TFEM$: Time-Frequency envelope misfit; FPM : Frequency-dependent phase misfit; TPM : Time-dependent phase misfit; $TFPM$: Time-Frequency phase misfit. Percentage values.). Left hand side: conforming model; Right hand side: non-conforming model.

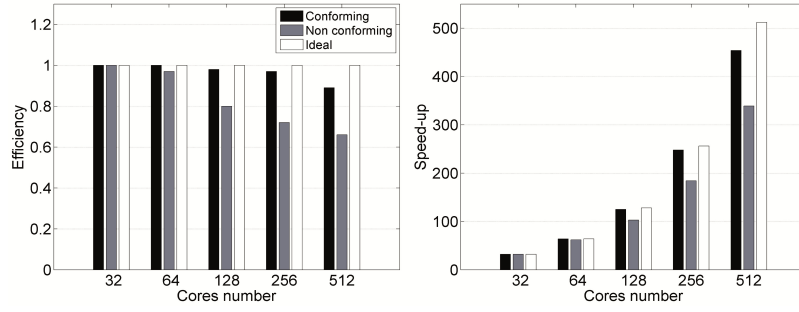


Figure 5: Performance of the parallel algorithm implemented in SPEED, in terms of efficiency and speed-up (total time), with reference to the conforming and non-conforming models (see Figure 3).

Table 3: Mechanical characteristics of the geological configuration, surrounding the Acquasanta bridge (see Figure 6).

		V_P [m/s]	V_S [m/s]	ρ [kg/m ³]	Q
Serpentino Jurassic		1100	635	2.400	125
		2300	1330	2800	150
Calcescisti Jurassic		1800	1200	2500	150
		2300	1330	2800	150
Alluvial Deposits		300	173	1925	25

As shown in Figure 6 and Figure 7, the considered problem, including both the structure and its surrounding area, involves very different spatial scales, from that of the geological model (hundreds of meters) to that of the bridge details (tens of centimeters). Two different meshes were constructed, one relying on a classical conforming spectral element approach, and another one using the non-conforming approach previously described. In particular, the need to accomplish the complex geometry of the Acquasanta viaduct and of the surrounding alluvial deposits as well implied, in the conforming approach, the adoption of a huge number of deformed elements up to the bottom of the model. Using a standard conforming mesh, indeed, such a multi-scale description can be obtained only through subsequent refinements, yielding a significant increase of the number of elements, a worsening of their quality and therefore the growth of the computational burden of the problem.

On the other hand, the non-conforming strategy enables significant advantages, namely:

- i) varying the mesh size and scheme (**h**-adaptivity) between the deep and outcropping rock layer, in order to drastically reduce the number of elements in that part of the model, as clearly showed in the top row of Figure 7.
- ii) varying the polynomial approximation degree (**N**-adaptivity) between the surface rock and the alluvial deposits, from $N = 4$ to $N = 3$, as sketched in the middle zoom of bottom row of Figure 6. In this way it is possible to reduce the number of unknowns of the problems, keeping the average element size of the elements inside the alluvial deposits smaller than those at outcropping bedrock.
- iii) varying both the mesh size and the polynomial approximation degree (**h**- and **N**-adaptivity) between the bridge and the rest of the model, as highlighted in the zooms of bottom row of Figure 6. In this case the structural elements of the viaduct are described by a larger number of elements, while the adoption of $N = 2$, instead of $N = 3$ (in the alluvial deposits) or $N = 4$ (at outcropping bedrock), does not increase excessively the computational costs of the analysis. It is worth remarking that, apart from the meshing strategy, there are no differences between the two numerical models in terms of model extension ($2 \times 1.75 \times 0.86 \text{ km}$), mechanical properties (Table 3) and seismic source. As regards the latter, a point double couple at 540 m depth was considered. As highlighted in Figure 6, the use of the non-conforming approach has allowed us to tailor the spatial discretization (**h**-adaptivity) and/or the local polynomial degree (**N**-adaptivity) to the different elements involved in a complex DSSI problem. This results in a non-conforming model having approximately the half of the elements of the conforming model. Furthermore, the hexahedral elements are characterized by a significant improvement of the quality metric (see Figure 7), and likely of the numerical solution.

Figure 8 shows a quantitative comparison between the velocity time-history obtained with the conforming and non-conforming models at a point located on the deck of the bridge (Receiver R in Figure 6), according to time-frequency misfit criteria proposed by [54]. An excellent agreement is found between the two solu-

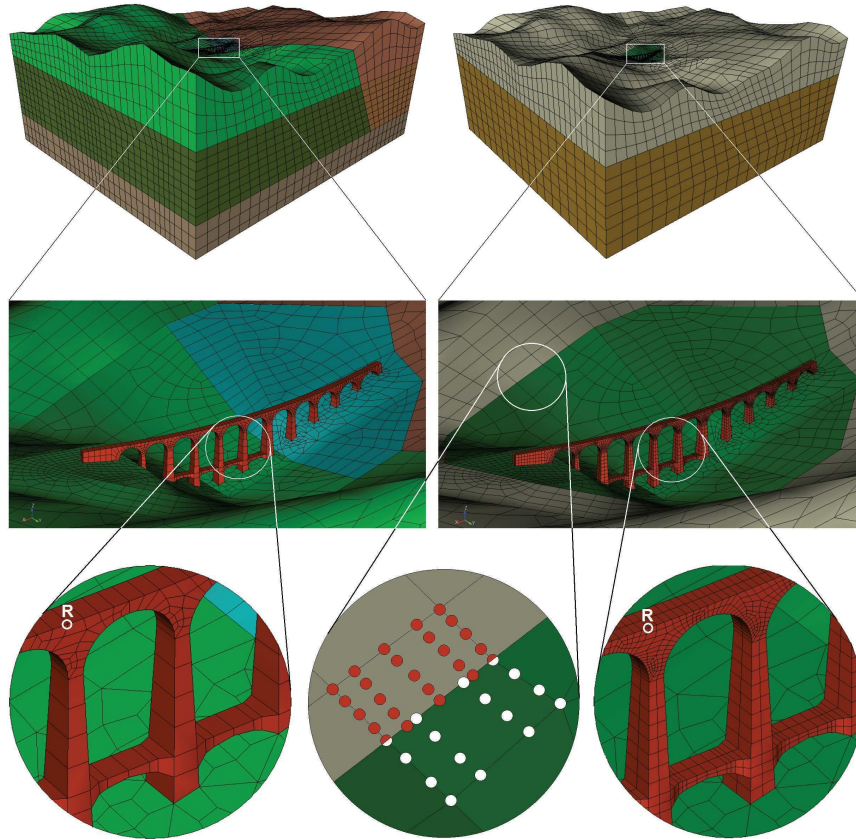


Figure 6: Progressive zoom of 3D models of Acquasanta bridge and the surrounding geological configuration. Left hand side: Conforming mesh in which different colors identify materials with different mechanical properties (see Table 3). Right hand side: Non-conforming mesh, in which different colors identify different sub-domains (\mathbf{h} - and \mathbf{N} - adaptivity), independently meshed and then combined. Letter \mathbf{R} denotes the location of the receiver adopted in the analysis.

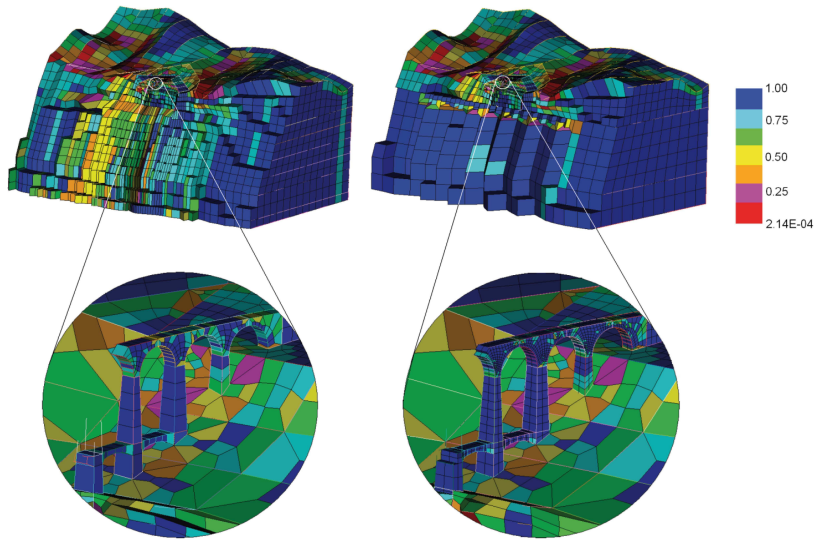


Figure 7: Transversal section of the two 3D models with zoom on the Acquasanta bridge. The non-conforming mesh (right hand side) is characterized by a lower number of hexahedra with a better level of quality metrics, here represented as a function of the scaled Jacobian of the element (with 1 meaning excellent quality).

tions confirming that the non-conforming approach preserves, or even improves, the accuracy of the solution. Some representative results of the numerical simulation are depicted in Figure 9 in terms of snapshots of the displacement of the Acquasanta bridge. It is possible to observe, through the snapshots, the movement of the deck and piers of the bridge.

4.3 The Christchurch Central Business District (CBD)

The second application of SPEED focuses on the simulation of the seismic response of the Central Business District (CBD), social and economic heart of the city of Christchurch, heavily damaged during the M_W 6.2 earthquake of 22 February 2011, characterized by a high density of tall buildings.

Between September 2010 and December 2011 the Canterbury Plains and, in particular, the city of Christchurch, in the South Island of New Zealand, experienced four major earthquakes, having M_W greater than 6.0 and a huge number of aftershocks [30]. On 22 February 2011, the most damaging and deadliest event of the seismic sequence, a M_W 6.2 earthquake, struck the city and the suburbs of Christchurch, causing extensive destruction and more than 180 victims. Beyond the causes and consequences of the event, different aspects drew the attention of the scientific community on this particular earthquake. Among them it is worth to emphasize: (i) the extremely severe strong ground-shaking observed [8], (ii) the widespread liquefaction phenomena across the city [17], and (iii) the

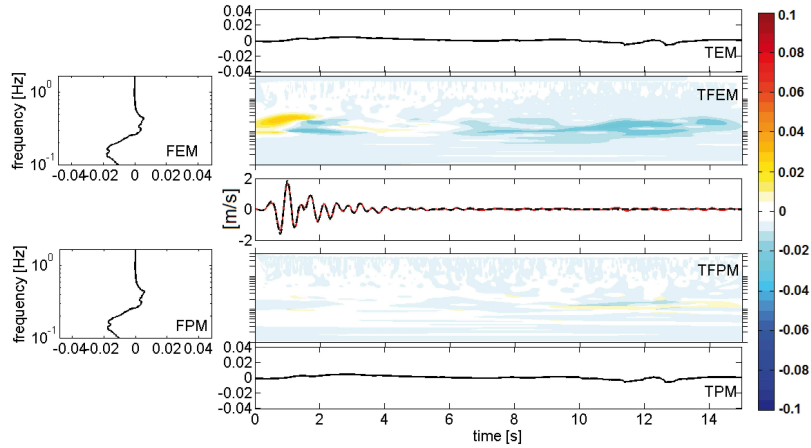


Figure 8: Time-frequency misfit according to [54] between the velocity time history obtained with the conforming and non-conforming models at the point \mathbf{R} located on the deck of the bridge (see Figure 6). FEM: Frequency-dependent envelope misfit; TEM: Time-dependent envelope misfit; TFEM: Time-Frequency envelope misfit; FPM: Frequency-dependent phase misfit; TPM: Time-dependent phase misfit; TFPM: Time-Frequency phase misfit.

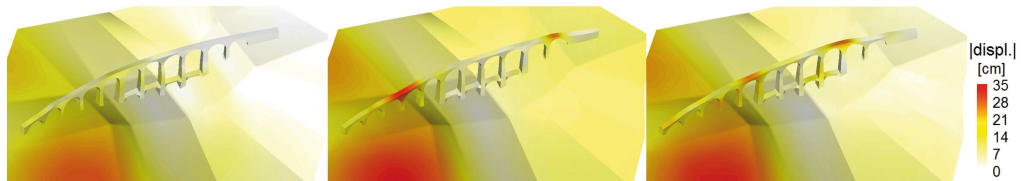


Figure 9: Snapshots ($t = 0.3, 0.6$ and 0.9 s, from left to right) of the simulated displacement of the Acquasanta viaduct. Displacements are considered in their absolute values. An amplification factor has been adopted for visualization purpose.

absence of evidence of the system of faults that generated the Canterbury seismic sequence, prior to the September 2010 M_W 7.1 Darfield event [34].

The main purpose of the application shown herein is the numerical evaluation, by a fully coupled approach, of seismic wave propagation effects from the earthquake source, to the local geological features, up to the densely urbanized area of Christchurch. In particular, a 3D model, encompassing both the regional and local urban scale, was constructed to study the wave passage effects on pounding-prone compounds of buildings as well as the influence of a densely urbanized area on the spatial variability of strong ground motion, and on the observed variability of damage in apparently homogeneous areas. In fact, a densely urbanized area located in an alluvial basin could affect the seismic wave field, both in a passive way, as the buildings and their foundations are obstacles to the seismic wave front, and in an active way, behaving like an extended surface source area, consisting of closely spaced sources of translational and rotational motions [85, 77, 83].

In this application, we exploit the non-conforming techniques, integrating the numerical model of the Canterbury Plains (see [36]) with a realistic inventory of buildings, namely, a set of around 150 buildings within the Christchurch CBD, as illustrated in Figure 10. As a starting point, the real configuration of the CBD has been considered, taking information on height and floor-plan dimensions of the buildings within an area having a dimension of about $1\text{ km} \times 1\text{ km}$. Also the foundations, for an average depth of 10 m , and the surrounding soil, for a depth of 50 m , have been taken into account. Assuming a mesh size of around 5 m , the CBD is described by a number of about 500000 hexahedral elements. The numerical mesh of the CBD has been successively included into the model of the Canterbury Plains, the latter having a global extension size $60\text{ km} \times 60\text{ km} \times 20\text{ km}$ and a number of around 500000 hexahedral elements with maximum size, at bedrock, of around 1.500 m , by enabling the contact between elements having, on one side, size of around 5 m (CBD model) and, on the other side, 50 m (Canterbury Plains), see Figure 10.

The resulting model reaches therefore a global number of hexahedral elements of more than one million. The buildings, modeled as homogeneous blocks, could be considered as shear beams, as recalled by different authors [85, 83]. According to [83], the following relation between V_S and the interstory height H_S can be obtained:

$$V_S = 28H_S. \quad (20)$$

Considering a typical interstory height of around 4 m , a value of V_S equal 100 m/s was adopted for the building material. A larger value of V_S , equal to 400 m/s , was adopted for the foundations, while $V_P = 2.5V_S$ was considered. The density and the quality factor Q of the buildings is equal to 300 kg/m^3 and 10, respectively. The latter, corresponds to a critical damping ratio $\xi = 0.05$. These values are in agreement with values adopted in other 2D studies (e.g. [90, 87]).

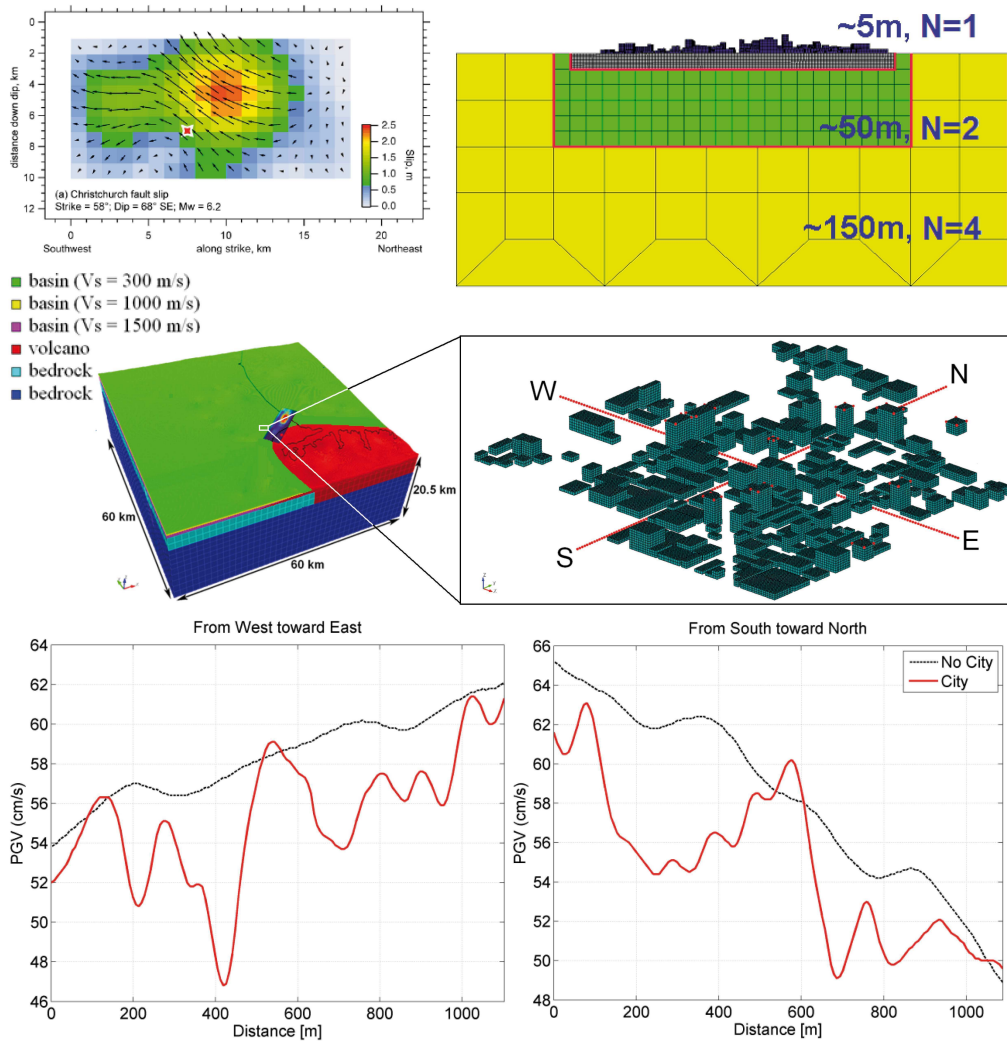


Figure 10: Peak Ground Velocity (PGV) along two representative directions across the CBD, namely West-East (W-E) and South-North (S-N), with (red line) or without (black line) the presence of the cluster of buildings. The distance between adjacent receivers is equal to 7.5 m. The multi-scale problem has been addressed through a non-conforming approach sketched in the top row, while the seismic source model has been adapted from a press release by the GNS (New Zealand Institute of Geological and Nuclear Sciences).

In order to evaluate the effect of the densely urbanized area of the CBD on the propagation of seismic waves, Figure 10 shows the Peak Ground Velocity (*PGV*) values, computed along two directions across the CBD, namely South-North (S-N) and East-West (E-W), with and without the presence of the buildings. It is noted that constructive and destructive interference between the building-foundation system and the surrounding soil may either reduce or amplify the ground motion, increasing the spatial variability of the surface response within the CBD. Looking at the variability of surface earthquake ground motion, it is worth noting the active role played by the buildings cluster, in substantial agreement with the words of Trifunac [85]: *this urban setting of buildings indeed is not merely an obstacle to the wave propagation field, but plays an active role, acting as an “extended surface source area consisting of a large number of closely spaced sources of translational and rotational motions”*.

To shed light on the issues regarding SCI effects, Figure 11 reports some snapshots of the simulated displacement wavefield, with particular reference to response of the CBD buildings. In this example, SCI turns out to produce scattering and focusing effects, increasing the ground motion variability within the CBD area, at a very small scale, and, hence, the consequent rotational motions at the base of the buildings themselves. Furthermore, these snapshots point out that pounding effects, related to the different vibration modes of the nearby buildings, are realistically reproduced by the numerical simulations.

5 Concluding remarks

In this work a new high performance spectral element code has been presented, namely SPEED (*SPectral elements in elastodynamics with Discontinuous Galerkin*) to approach the 3D modeling of complex seismic scenarios. Relying on non-conforming high order spectral elements, suitable for handling non-matching grids as well as variable approximation orders, the code has been proved to be capable of accommodating sharp discontinuities or difficult geometrical constraints in an extremely efficient and versatile way. This capability turns out to be extremely useful in a variety of practical seismic engineering wave propagation problems. After checking the accuracy of the proposed technique through a classical benchmark, a couple of challenging engineering applications has been presented. The seismic response of a railway viaduct under complex geotechnical setting is a meaningful example of how SPEED could easily deal with advances dynamic soil structure interaction (DSSI) problems. The second case study could be considered even more challenging, aiming at studying the seismic response of the central business district (CBD) of Christchurch, located in the alluvial plain of Canterbury in New Zealand. The recent seismic sequence, started with the Darfield earthquake in September 2010 and endured several months, caused more than 180 casualties and devastated the entire region. We focused on the most devastating event of the whole sequence, namely the Lyttleton event (22

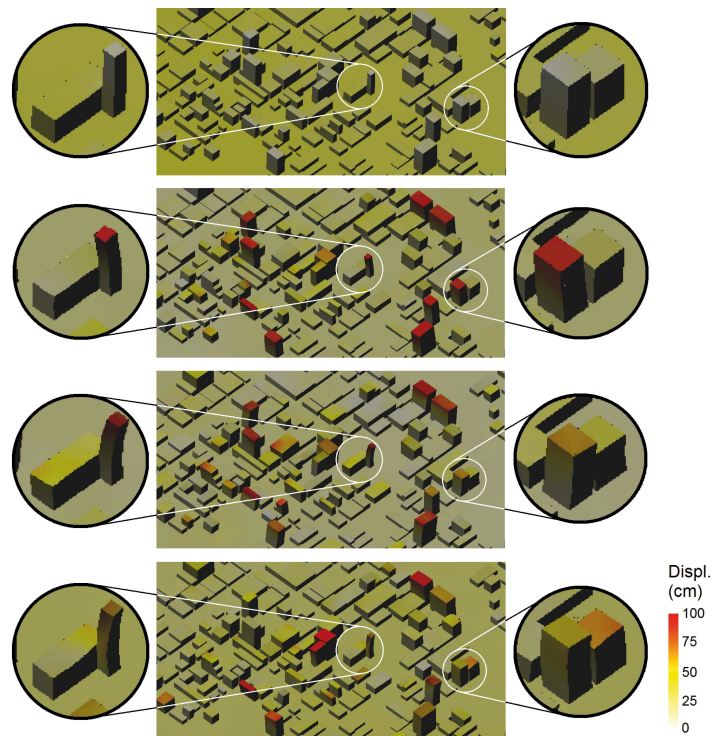


Figure 11: Snapshots ($t = 6, 8, 10$ and 12 s, from top to bottom) of the simulated displacement of the buildings of the CBD, with zoom on significant structures or compounds. Displacements are considered in their absolute values. On the ground, between buildings, is visible the displacement wave-field. An amplification factor has been adopted for visualization purpose.

February 2011), simulating the kinematic rupture along the fault and studying the wave propagation through the complex deep soft sediments up to the high and middle rise buildings located inside the CBD of Christchurch. Both these application examples showed that SPEED may enable great advantages for modeling complex multi-scale seismic scenario, by relaxing certain constraints imposed by standard conforming SE methods and, therefore, reducing the efforts devoted to the mesh creation preserving, however the accuracy of spectral approximations.

Acknowledgements

The work has been performed under the HPC-EUROPA2 project (project number: 228398) with the support of the European Commission - Capacities Area - Research Infrastructures. The authors warmly thank Alfio Quarteroni, Roberto Paolucci, Paola F. Antonietti and Francesca Rapetti; this work largely benefits from their comments and suggestions. The authors are very grateful to CINECA-CILEA, in particular to Paride Dagna and Paolo Ramieri for allowing the extensive use of the Lagrange cluster and for providing technical assistance. Finally, the authors extend their gratitude to Dimitri Komatitsch for the critical remarks that have contributed to improve the quality of the paper.

References

- [1] Adams R.A., Fournier J.F.F. 2003. *Sobolev Spaces* (2nd edn). Academic Press.
- [2] Antonietti P.F., Mazzieri I., Quarteroni A., Rapetti F. 2012. *Non-conforming high order approximations of the elastodynamics equation*. Computer Methods in Applied Mechanics and Engineering, **209-212**: 212–238.
- [3] Arnold D.N., Brezzi F., Cockburn B., Marini L.D. 2001/02. *Unified analysis of discontinuous Galerkin methods for elliptic problems*. SIAM Journal of Numerical Analysis, **39**(5): 1749–1779.
- [4] Arnold D.N. 1982. *An interior penalty finite element method with discontinuous elements*. SIAM Journal on Numerical Analysis, **19**(4): 742–760.
- [5] Babuska I., Szabo B.A., Katz I.N. 1981. *The p-version of the finite element method*. SIAM Journal of Numerical Analysis, **18**: 512–545.
- [6] Babuska I., Suri M. 1987. *The hp-version of the finite element method with quasiuniform meshes*. ESAIM: Mathematical Modelling and Numerical Analysis, **21**(2): 199–238.

- [7] Bielak J., Graves R.W., Olsen K.B., Taborda R., Ramirez-Guzman L., Day S.M., Ely G.P., Roten D., Jordan T.H., Maechling P.J., Urbanic J., Cui Y., Juve G. 2010. *The ShakeOut earthquake scenario: Verification of three simulation sets*. Geophysical Journal International, **180**: 375–404.
- [8] Bradley B.A., Cubrinovski M. 2011. *Near-source strong ground motions observed in the 22 February 2011 Christchurch earthquake*. Seismological Research Letters, **82**(6): 853–865.
- [9] Casadei F., Gabellini E., Fotia G., Maggio F., Quarteroni A. 2002. *A mortar spectral/finite element method for complex 2D and 3D elastodynamic problems*. Computer Methods in Applied Mechanics and Engineering, **191**(45): 5119–5148.
- [10] Chaljub E., Capdeville Y., Vilotte J.P. 2003. *Solving elastodynamics in a fluid-solid heterogeneous sphere: a parallel spectral element approximation on non-conforming grids*. Journal of Computational Physics, **187**(2): 457–491.
- [11] Chaljub E., Komatitsch D., Vilotte J.P., Capdeville Y., Valette B., Festa G. 2007. *Spectral element analysis in seismology*. Advances in wave propagation in heterogeneous media, volume 48 of Advances in Geophysics, pages 365–419. Elsevier-Academic Press.
- [12] Chaljub E., Moczo P., Tsuno S, Bard P.Y., Kristek J., Käser M., Stupazzini M., Kristekova M. 2010. *Quantitative comparison of four numerical predictions of 3D ground motion in the Grenoble valley, France*. Bulletin of the Seismological Society of America, **100**(4): 1427–1455.
- [13] Chung E.T., Engquist B. 2006. *Optimal discontinuous Galerkin methods for wave propagation*. SIAM Journal on Numerical Analysis, **44**: 2131–2158.
- [14] Canuto C., Hussaini M.Y., Quarteroni A., Zang T.A. 2006. *Spectral methods - Fundamentals in single domains*. Springer-Verlag.
- [15] Clayton R., Engquist B. 1977. *Absorbing boundary conditions for acoustic and elastic wave equations*. Bulletin of the Seismological Society of America, **67**: 1529–1540.
- [16] Cockburn B., Karniadakis G.E., Shu C.W. 2000. *Discontinuous Galerkin Methods: Theory, Computation and Applications*. Springer-Verlag.
- [17] Cubrinovski M., Bray J.D., Taylor M., Giorgini S., Bradley B., Wotherpoon L., Zupan J. 2011. *Soil liquefaction effects in the central business district during the February 2011 Christchurch earthquake*. Seismological Research Letters, **82**(6): 893–904.

- [18] Day S.M., Bradley C.R. 2001. *Memory-efficient simulation of anelastic wave propagation*. Bulletin of the Seismological Society of America, **91**(3): 520–531.
- [19] Day S.M., Graves R., Bielak J., Dreger D., Larsen S., Olsen K.B., Pitarka A., Ramirez-Guzman L. 2008. *Model for Basin Effects on Long-Period Response Spectra in Southern California*. Earthquake Spectra, **24**(1): 257–277.
- [20] De Basabe J.D., Sen M.K. 2010. *Stability of the highorder finite elements for acoustic or elastic wave propagation with high order time stepping*. Geophysical Journal International, **181**(1): 577–590.
- [21] De Basabe J.D., Sen M.K., Wheeler M.F. 2008. *The interior penalty discontinuous Galerkin method for elastic wave propagation: grid dispersion*. Geophysical Journal International, **175**(1): 83–93.
- [22] De Basabe J.D., Sen M.K. 2007. *Grid dispersion and stability criteria of some common finite element methods for acoustic and elastic wave equations*. Geophysics, **72**(6): T81–T95.
- [23] De la Puente J., Käser M., Dumbser M., Igel H. 2007. *An arbitrary high order Discontinuous Galerkin method for elastic waves on unstructured meshes IV: Anisotropy*. Geophysical Journal International, **169**(3): 1210–1228.
- [24] Dumbser M., Käser M., Toro E.F. 2007. *An arbitrary high-order Discontinuous Galerkin method for elastic waves on unstructured meshes V: Local time stepping and p-adaptivity*. Geophysical Journal International, **171**(2): 695–717.
- [25] Faccioli E., Maggio F., Paolucci R., Quarteroni A. 1997. *2D and 3D elastic wave propagation by a pseudo-spectral domain decomposition method*. Journal of Seismology, **1**(3): 237–251.
- [26] Falk R.S., Richter G.R. 1999. *Explicit finite element methods for symmetric hyperbolic equations*. SIAM Journal on Numerical Analysis, **36**(3): 935–952.
- [27] Fichtner A. 2010. *Full Seismic Waveform Modelling and Inversion* Springer-Verlag.
- [28] Giraldo F.X., Hesthaven J.S., Warburton T. 2002. *Nodal high order discontinuous Galerkin methods for the spherical shallow water equations*. Journal of Computational Physics, **181**(2): 499–525.
- [29] Givoli D. 1991. *Non-reflecting boundary conditions*. Journal of Computational Physics **94**: 1–29.

- [30] Gledhill K., Ristau J., Reyners M., Fry B., Holden C. 2011. *The Darfield (Canterbury, New Zealand) M_W 7.1 earthquake of September 2010: A preliminary seismological report*. Seismological Research Letters, **82**(3): 378–386.
- [31] Graves R.W. 1996. *Simulating seismic wave propagation in 3D elastic media using staggered-grid finite differences*. Bulletin of the Seismological Society of America, **86**(4): 1091–1106.
- [32] Graves R.W., Aagaard B.T., Hudnut K.W., Star L.M., Stewart J.P., Jordan T.H. 2008. *Broadband simulations for M_W 7.8 Southern San Andreas earthquakes: Ground motion sensitivity to rupture speed*. Geophysical Research Letters, **35**: L22302, doi:10.1029/2008GL035750.
- [33] Graves R.W., Jordan T., Callaghan S., Deelman E., Field E., Juve G., Kesselman C., Maechling P., Mehta G., Milner K., Okaya D., Small P., Vahi K. 2010. *CyberShake: A physics-based seismic hazard model for Southern California*. Pure and Applied Geophysics, **168**(3-4): 367–381.
- [34] Green A.G., Campbell F.M., Kaiser A.E., Dorn C., Carpentier S., Doetsch J.A., Horstmeyer H., Nobes D., Campbell J., Finnemore M., 2010. *Seismic reflection images of active faults on New Zealand’s South Island*. Fourth International Conference on Environmental and Engineering Geophysics, Chengdu, China.
- [35] Grote M.J., Schneebeli A., Schötzau D. 2006. *Discontinuous Galerkin finite element method for the wave equation*. SIAM Journal of Numerical Analysis, **44**(6): 2408–2431.
- [36] Guidotti R., Stupazzini M., Smerzini C., Paolucci R., Ramieri P. 2011. *Numerical study on the role of basin geometry and kinematic seismic source in 3D ground motion simulation of the 22 February 2011 M_W 6.2 Christchurch earthquake*. Seismological Research Letters, **82**(6): 767–782.
- [37] Guidotti R. 2012. *Near-field earthquake ground motion rotations and relevance on civil engineering structures*. Ph.D. Thesis, Politecnico di Milano.
- [38] Hesthaven J.S., Warburton T. 2008. *Nodal discontinuous Galerkin methods*. Springer-Verlag.
- [39] Hu F.Q., Hussaini M.Y., Rasetarinera P. 1999. *An analysis of the discontinuous Galerkin method for wave propagation problems*. Journal of Computational Physics, **151**(2): 921–946.
- [40] Isbilibiroglu Y., Taborda R., Bielak J. 2013. *Coupled soil-structure interaction effects of building clusters during earthquakes*. Earthquake Spectra, Submitted for publication.

- [41] Jones L.M., Bernknopf R., Cox D., Goltz J., Hudnut K., Mileti D., Perry S., Ponti D., Porter K., Reichle M., Seligson H., Shoaf K., Treiman J., Wein A. 2008. *The ShakeOut scenario*. Technical Report USGS-R1150, U.S. Geological Survey and California Geological Survey.
- [42] Käser M., Dumbser M. 2006. *An arbitrary high order Discontinuous Galerkin method for elastic waves on unstructured meshes I: The two-dimensional isotropic case with external source terms*. Geophysical Journal International, **166**(2): 855–877.
- [43] Käser M., Dumbser M., De La Puente J., Igel H. 2007. *An arbitrary high-order Discontinuous Galerkin method for elastic waves on unstructured meshes III: Viscoelastic attenuation*. Geophysical Journal International, **168**(1): 224–242.
- [44] Kim E., Bielak J., Ghattas O. 2003. *Large-scale Northridge earthquake simulation using octree-based multi-resolution mesh method*. In 16th ASCE Engineering Mechanics Conference, University of Washington, Seattle.
- [45] Klöckner A., Warburton T., Bridge J., Hesthaven J.S. 2009. *Nodal discontinuous Galerkin methods on graphics processors*, Journal of Computational Physics, **228**: 7863–7882.
- [46] Komatitsch D., Göldeke D., Erlebacher G., Michéa D. 2010. *Modeling the propagation of elastic waves using spectral elements on a cluster of 192 GPUs*. Computer Science Research and Development, **25**(12): 75–82.
- [47] Komatitsch D. 2011. *Fluid solid coupling on a cluster of GPU graphics cards for seismic wave propagation*. Comptes Rendus de l’Académie des Sciences. Série IIb. Mécanique, **339**: 125–135.
- [48] Komatitsch D., Vilotte J.P. 1998 *The spectral element method: An efficient tool to simulate the seismic response of 2D and 3D geological structures*. Bulletin of the Seismological Society of America, **88**(2): 368–392.
- [49] Komatitsch D., Tromp J. 1999. *Introduction to the spectral-element method for 3-D seismic wave propagation*. Geophysical Journal International, **139**(3): 806–822.
- [50] Komatitsch D., Ritsema J., Tromp J. 2002. *The spectral-element method, Beowulf computing, and global seismology*. Science, **298**(5599): 1737–1742.
- [51] Komatitsch D., Liu Q., Tromp J., Suss P., Stidham C., Shaw J.H. 2004. *Simulations of ground motion in the Los Angeles Basin based upon the Spectral Element Method*. Bulletin of the Seismological Society of America, **94**(1): 187–206.

- [52] Kosloff D., Kessler D., Filho A.Q., Tessmer E., Behle A., Strahilevitz R. 1990. *Solution of the equation of dynamic elasticity by a Chebyshev spectral method*. Geophysics, **55**: 748–754.
- [53] Kosloff R., Kosloff D. 1986. *Absorbing boundaries for wave propagation problems*. Journal of Computational Physics, **63**(2): 363–376.
- [54] Kristekova M., Kristek J., Moczo P., Day S.M. 2006. *Misfit criteria for quantitative comparison of seismograms*. Bulletin of the Seismological Society of America, **96**(5): 1836–1850.
- [55] Lahaye D.J.P., Maggio F., Quarteroni A. 1997. *Hybrid finite element-spectral element approximation of wave propagation problems*. East-West Journal of Numerical Mathematics, **5**(4): 265–289.
- [56] Krishnan S., Ji C., Komatitsch D., Tromp J. 2006. *Case studies of damage to tall steel moment-frame buildings in Southern California during large San Andreas earthquakes*. Bulletin of the Seismological Society of America, **96**(4A): 1523–1537.
- [57] Kopriva D.A. 2006. *Metric identities and the discontinuous spectral element method on curvilinear meshes*. Journal of Scientific Computing, **26**(3): 301–327.
- [58] Kopriva D.A., Woodruff S.L., Hussaini M.Y. 2002. *Computation of electromagnetic scattering with a non conforming discontinuous spectral element method*. International Journal for Numerical Methods in Engineering, **53**(1): 105–122.
- [59] Maday Y., Patera A.T. 1989. *Spectral element methods for the incompressible Navier-Stokes equations*. in State of the Art Survey in Computational Mechanics A.K. Noor and J.T. Oden (Editors) ASME: 71–143.
- [60] Martin R., Komatitsch D., Gedney S.D. 2008. *A variational formulation of a stabilized unsplit convolutional perfectly matched layer for the isotropic or anisotropic seismic wave equation*. Computer Modeling in Engineering and Sciences, **37**(3): 274–304.
- [61] Mazzieri I. 2012. *Non-conforming high order methods for the elastodynamics equation*. PhD. Thesis, Politecnico di Milano.
- [62] Mercerat E.D., Vilotte J.P., Sanchez-Sesma F.J., 2006. *Triangular spectral-element simulation of two-dimensional elastic wave propagation using unstructured triangular grids*. Geophysical Journal International, **166**(2): 679–698.
- [63] Monk P., Richter G.R., 2005. *A discontinuous Galerkin method for linear symmetric hyperbolic systems in inhomogeneous media*. Journal of Scientific Computing, **22–23**: 443–477.

- [64] Olsen K.B., Archuleta R.J. 1996. *Three-dimensional simulation of earthquakes on the Los Angeles fault system*. Bulletin of the Seismological Society of America, **86**(3): 575–596.
- [65] Olsen K.B. 2001. *Three-dimensional ground motion simulations for large earthquakes on the San Andreas fault with dynamic and observational constraints*. Journal of Computational Acoustics, **9**(3): 1203–1214.
- [66] Olsen K.B., Day S.M., Dalguer L.A., Mayhew J., Cui Y., Zhu J., Cruz-Atienza V.M., Roten D., Maechling P., Jordan T.H., Okaya D., Chourasia A. 2009. *'ShakeOut-D: Ground motion estimates using an ensemble of large earthquakes on the southern San Andreas fault with spontaneous rupture propagation*. Geophysical Research Letters, **36**: L04303, doi:10.1029/2008GL036832.
- [67] Patera A.T. 1984. *A spectral element method for fluid dynamics: laminar flow in a channel expansion*. Journal of Computational Physics, **54**: 468–488.
- [68] Peter D., Komatitsch D., Luo Y., Martin R., Le Goff N., Casarotti E., Le Locher P., Magnoni F., Liu Q., Blitz C., Nissen Meyer T., Basini P., Tromp J. 2011. *Forward and adjoint simulations of seismic wave propagation on fully unstructured hexahedral meshes*. Geophysical Journal International, **186**(2): 721–739.
- [69] Petersen S., Farhat C., Tezaur R. 2009. *A space–time discontinuous Galerkin method for the solution of the wave equation in the time domain*. International Journal for Numerical Methods in Engineering, **78**(3): 275–295.
- [70] Priolo E., Carcione J.M., Seriani G. 1994. *Numerical simulation of interface waves by high-order spectral modeling techniques*. J. Acoust. Soc. Am. **95**(2): 681–693.
- [71] Quarteroni A., Sacco R., Saleri F. 2007. *Numerical mathematics* (2nd edn). Springer-Verlag.
- [72] Raviart P.A., Thomas J.M. 1983. *Introduction à l'analyse numérique des équations aux dérivées partielles*. Masson.
- [73] Reed W.H., Hill T.R. 1973. *Triangular mesh methods for the neutron transport equation*. Technical Report LAUR73479, Los Alamos Scientific Laboratory, Los Alamos, USA.
- [74] Rivière B., Shaw S., Wheeler M.F., Whiteman J.R. 2003. *Discontinuous Galerkin finite element methods for linear elasticity and quasistatic linear viscoelasticity*. Numerische Mathematik, **95**(2): 347–376.

- [75] Rivière B., Wheeler M.F. 2003. *Discontinuous finite element methods for acoustic and elastic wave problems*. Current trends in scientific computing, volume 329 of Contemporary Mathematics, pages 271-282. American Mathematical Society.
- [76] Rivière B. 2008. *Discontinuous Galerkin methods for solving elliptic and parabolic equations - Theory and implementation*. Society for Industrial and Applied Mathematics (SIAM).
- [77] Semblat J.F., Kham M., Bard P.Y. 2008. *Seismic wave propagation in alluvial basins and influence of site-city interaction*. Bulletin of the Seismological Society of America, **96**(6): 2665–2678.
- [78] Seriani G., Priolo E., Pregarz A. 1995. *Modelling waves in anisotropic media by a spectral element method*. Proceedings of the third international conference on mathematical and numerical aspects of wave propagation: 289–298. SIAM.
- [79] 4 M Service SpA 1998. *Analisi dei ponti ad arco della linea ferroviaria Genova-Ovada*. Survey on behalf of Ferrovie dello Stato, Genoa.
- [80] Stacey R. 1988. *Improved transparent boundary formulations for the elastic-wave equation*. Bulletin of the Seismological Society of America, **78**(6): 2089–2097.
- [81] Stupazzini M. 2004. *A spectral element approach for 3D dynamic soil-structure interaction problems*. Ph.D. Thesis, Politecnico di Milano.
- [82] Stupazzini M., Paolucci R., Igel H. 2009. *Near-fault earthquake ground-motion simulation in Grenoble Valley by high-performance spectral element code*. Bulletin of the Seismological Society of America, **99**(1): 286–301.
- [83] Taborda R., Bielak J. 2011. *Large-Scale Earthquake Simulation: Computational Seismology and Complex Engineering Systems*. Computing in Science and Engineering, **13**(4): 14–27.
- [84] Taborda R., Bielak J., Restrepo D. 2012. *Modeling 3D nonlinear soil effects in large-scale earthquake ground motion simulations*. Seismological Research Letters, **83**(6): In press.
- [85] Trifunac M.D. 2009. *The role of strong motion rotations in the response of structures near earthquake faults*. Soil Dynamics and Earthquake Engineering, **29**(2): 382–393.
- [86] Tromp J., Komatitsch D., Liu Q. 2008. *Spectral element and adjoint methods in seismology*. Communications in Computational Physics, **3**(1): 1–32.
- [87] Tsogka C., Wirgin A. 2003. *Simulation of seismic response in an idealized city*. Soil Dynamics and Earthquake Engineering, **23**(5): 391–402.

- [88] Wald D.J., Graves R.W. 1998. *The seismic response of the Los Angeles basin, California*. Bulletin of the Seismological Society of America, **88**(2): 337–356.
- [89] Wilcox L.C., Stadler G., Burstedde C., Ghattas O. 2010. *A high-order discontinuous Galerkin method for wave propagation through coupled elastic and acoustic media*. Journal of Computational Physics, **229**(24): 9373–9396.
- [90] Wirgin A., Bard P.Y. 1996. *Effects of buildings on the duration and amplitude of ground motion in Mexico City*. Bulletin of the Seismological Society of America, **86**(3): 914–920.

MOX Technical Reports, last issues

Dipartimento di Matematica “F. Brioschi”,
Politecnico di Milano, Via Bonardi 9 - 20133 Milano (Italy)

- 24/2013** MAZZIERI, I.; STUPAZZINI, M.; GUIDOTTI, R.; SMERZINI, C.
SPEED-Spectral Elements in Elastodynamics with Discontinuous Galerkin: a non-conforming approach for 3D multi-scale problems
- 23/2013** SRENSSEN, H.; GOLDSMITH, J.; SANGALLI, L.M.
An introduction with medical applications to functional data analysis
- 22/2013** FALCONE, M.; VERANI, M.
Recent Results in Shape Optimization and Optimal Control for PDEs
- 21/2013** PEROTTO, S.; VENEZIANI, A.
Coupled model and grid adaptivity in hierarchical reduction of elliptic problems
- 20/2013** AZZIMONTI, L.; NOBILE, F.; SANGALLI, L.M.; SECCHI, P.
Mixed Finite Elements for spatial regression with PDE penalization
- 19/2013** AZZIMONTI, L.; SANGALLI, L.M.; SECCHI, P.; DOMANIN, M.; NOBILE, F.
Blood flow velocity field estimation via spatial regression with PDE penalization
- 18/2013** DISCACCIATI, M.; GERVASIO, P.; QUARTERONI, A.
Interface Control Domain Decomposition (ICDD) Methods for Coupled Diffusion and Advection-Diffusion Problems
- 17/2013** CHEN, P.; QUARTERONI, A.
Accurate and efficient evaluation of failure probability for partial differential equations with random input data
- 16/2013** FAGGIANO, E. ; LORENZI, T. ; QUARTERONI, A.
Metal Artifact Reduction in Computed Tomography Images by Variational inpainting Methods
- 15/2013** ANTONIETTI, P.F.; GIANI, S.; HOUSTON, P.
Domain Decomposition Preconditioners for Discontinuous Galerkin Methods for Elliptic Problems on Complicated Domains